AD-A108 266 AIR FORCE WRIGHT AERONAUTICAL LABS WRIGHT-PATTERSON AFB OH F/G 9/1
MEASURED PULSE TRANSFER CHARACTERISTICS OF HIGH IMPEDANCE MICRO--ETC(U)
APR 81 D G MCLAINE
UNCLASSIFIED AFWAL-TR-80-1160 NL

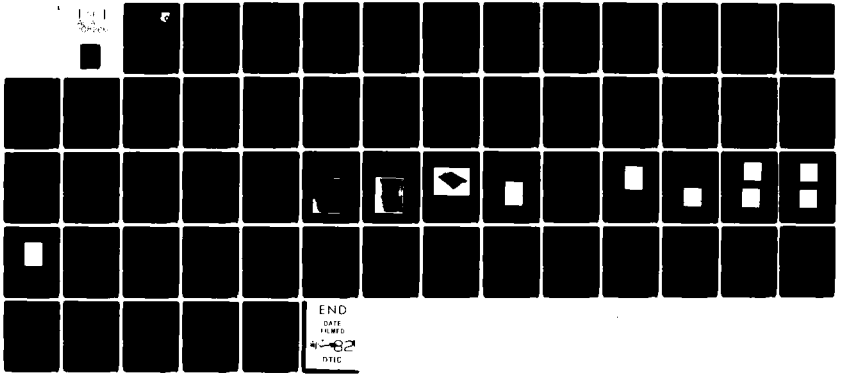

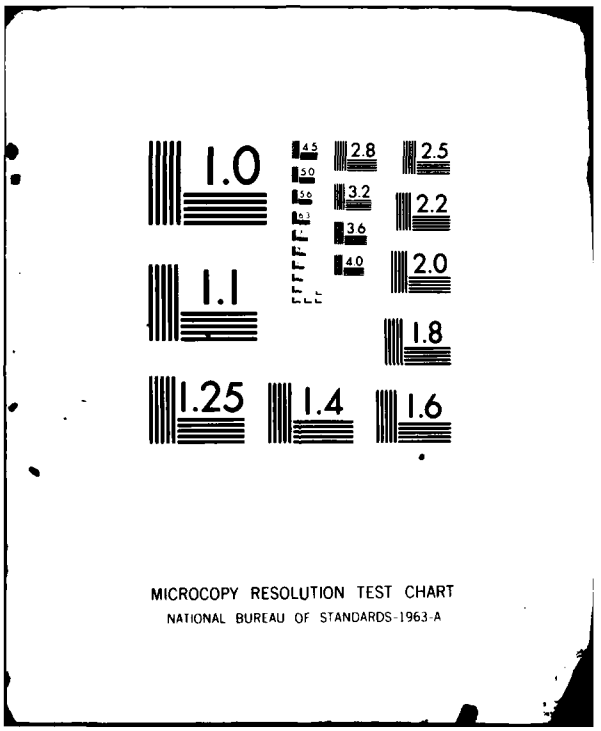
1.0
1.1
1.25
1.4
1.6
1.8
2.0
2.2
2.5
2.8
3.2
3.6
4.0
4.5
5.0
5.6
MICROCOPY RESOLUTION TEST CHART
NATIONAL BUREAU OF STANDARDS-1963-A

(12) LEVEL II

AFWAL-TR-80-1160

AD A108266

MEASURED PULSE TRANSFER CHARACTERISTICS OF HIGH IMPEDANCE MICROSTRIP LINES

APRIL 1981

FINAL REPORT FOR PERIOD MARCH 1979 — MARCH 1980

Approved for public release; distribution unlimited

AVIONICS LABORATORY
AIR FORCE WRIGHT AERONAUTICAL LABORATORIES
AIR FORCE SYSTEMS COMMAND
WRIGHT-PATTERSON AIR FORCE BASE, OHIO 45433

NOTICE

When Government drawings, specifications, or other data are used for any purpose other than in connection with a definitely related Government procurement operation, the United States Government thereby incurs no responsibility nor any obligation whatsoever; and the fact that the government may have formulated, furnished, or in any way supplied the said drawings, specifications, or other data, is not to be regarded by implication or otherwise as in any manner licensing the holder or any other person or corporation, or conveying any rights or permission to manufacture, use, or sell any patented invention that may in any way be related thereto.

This report has been reviewed by the Office of Public Affairs (ASD/PA) and is releasable to the National Technical Information Service(NTIS). At NTIS, it will be available to the general public, including foreign nations.

This technical report has been reviewed and is approved for publication.

DAVID G. MCLAINE, Project Engineer
Design & Packaging Group

J.B. RAWLINGS, Capt, USAF
Chief, Design & Packaging Group

STANLEY E. WAGNER, Chief
Microelectronics Branch
Electronic Technology Division

"If your address has changed, if you wish to be removed from our mailing list, or if the addressee is no longer employed by your organization please notify AFWAL/AADE-3, W-PAFB, OH 45433 to help us maintain a current mailing list".

Copies of this report should not be returned unless return is required by security considerations, contractual obligations, or notice on a specific document.

SECURITY CLASSIFICATION OF THIS PAGE *(When Data Entered)*

REPORT DOCUMENTATION PAGE

READ INSTRUCTIONS BEFORE COMPLETING FORM

1. REPORT NUMBER: AFWAL-TR-80-1160	2. GOVT ACCESSION NO.: AD-A108 266
3. RECIPIENT'S CATALOG NUMBER:	
4. TITLE *(and Subtitle)*: MEASURED PULSE TRANSFER CHARACTERISTICS OF HIGH IMPEDANCE MICROSTRIP LINES	5. TYPE OF REPORT & PERIOD COVERED: FINAL MAR79 - MAR80
	6. PERFORMING ORG. REPORT NUMBER:
7. AUTHOR(s): David G. McLaine	8. CONTRACT OR GRANT NUMBER(s):
9. PERFORMING ORGANIZATION NAME AND ADDRESS: Avionics Laboratory (AFWAL/AADE) Air Force Wright Aeronautical Laboratories Wright-Patterson AFB OH 45433	10. PROGRAM ELEMENT, PROJECT, TASK AREA & WORK UNIT NUMBERS: 60964201
11. CONTROLLING OFFICE NAME AND ADDRESS: Avionics Laboraotry (AFWAL/AADE) Air Force Wright Aeronautical Laboratories Wright Patterson AFB OH 45433	12. REPORT DATE: April 1981
	13. NUMBER OF PAGES: 58
14. MONITORING AGENCY NAME & ADDRESS *(if different from Controlling Office)*:	15. SECURITY CLASS. *(of this report)*: UNCLASSIFIED
	15a. DECLASSIFICATION/DOWNGRADING SCHEDULE:

16. DISTRIBUTION STATEMENT *(of this Report)*

Approved for public release; distribution unlimited.

17. DISTRIBUTION STATEMENT *(of the abstract entered in Block 20, if different from Report)*

18. SUPPLEMENTARY NOTES

19. KEY WORDS *(Continue on reverse side if necessary and identify by block number)*

Microstrip
Digital Pulse Transmission
Thick Film Technology
High Speed Digital Circuits

20. ABSTRACT *(Continue on reverse side if necessary and identify by block number)*

Theoretical and experimental results of the propagation and coupling characteristics of fast risetime (50-150 ps) digital pulses on high impedance (100 ohm) microstrip lines are presented. Theoretical microstrip design equations are discussed and the significance of dispersion analyzed. Five mil lines on 35 mil alumina substrates were fabricated using standard thick film technology. Various line lengths, coupled line lengths, and coupled line spacings were analyzed to determine pulse degradation effects and the coupling coefficients between lines.

DD FORM 1 JAN 73 1473 EDITION OF 1 NOV 65 IS OBSOLETE

SECURITY CLASSIFICATION OF THIS PAGE *(When Data Entered)*

TABLE OF CONTENTS

LIST OF ILLUSTRATIONS

LIST OF ILLUSTRATIONS (Cont'd)

LIST OF ILLUSTRATIONS (Cont'd)

LIST OF TABLES

1.0 INTRODUCTION

Digital semiconductor device technology is advancing in two non-exclusive primary directions. Levels of integration (gates/cm^2) are increasing; and, gate propagation delays are decreasing. The methodology for interconnecting Integrated Circuit (IC) chips is becoming very important. Controlled impedance lines are often required and the transfer characteristics of these lines will ultimately determine the maximum circuit operational speed. Line spacing will have a significant impact on interconnect density, achievable circuit complexity, and fabrication cost. In addition, the line characteristic impedance levels will determine chip drive requirements and the resulting power dissipation levels. Approaches currently used for interconnecting high-speed, high-density IC chips include multilayer printed wiring boards, thin films (evaporated metals) on ceramics, green tape co-fired ceramic substrates, and thick films (screen printed conductor and dielectric inks) on ceramics.

This study is limited to the evaluation/characterization of thick film ceramic substrates. This choice was based on practical considerations which include the availability of materials and processing capabilities. Microstrip line geometry was selected as the only viable approach to achieve line characteristic impedances in the 100 ohm range. Five (5) mil lines were screened and fired on 35 mil alumina substrates and evaluated in terms of the signal transfer characteristics. In addition to analyzing the loss and dispersion characteristics of single lines, coupling experiments were conducted to determine the coupling coefficients between lines under various conditions. All experimental data was derived using a fast risetime step function generator to

simulate the leading edge of a high speed digital logic pulse.

2.0 DISCUSSION OF MICROSTRIP TRANSMISSION LINES

Microstrip circuits have been studied and analyzed by a large number of investigators during the 1960's and early 1970's. Papers written by these investigators are now being consolidated by authors such as K. C. Gupta, Ramesh Garg, and I. J. Bahl[1]. Most of these papers deal with the microwave transmission characteristics of microstrip by analyzing parameters such as characteristic impedance, effective dielectric constant, conductor and dielectric losses, radiation loss, dispersion, higher order moding, matching and coupling techniques, etc. Although much of this published data is beneficial in understanding microstrip lines when used to interconnect high speed digital logic circuits, the design equations presented cannot be used directly because of the frequency dependence of various parameters.

The pulses of interest for this study have rise and fall times in the 50 to 150 picosecond range and thus exhibit frequency components well above 10.0 GHz. This extremely wide bandwidth is difficult to handle even with an ideal TEM mode transmission structure. Microstrip structures on the other hand are desirable from the standpoint of ease of fabrication since all the design is done on the plane of the conductors. These structures have been used quite successfully at frequencies well above 10.0 GHz; however, since signals propagate in a quasi-TEM mode, some dispersion does exist that will cause at least some pulse degradation. A pure TEM mode will not propagate on a microstrip line because the phase velocity in the air dielectric is faster than in the substrate and all fields are not confined to the substrate. Proof of this is given in [1].

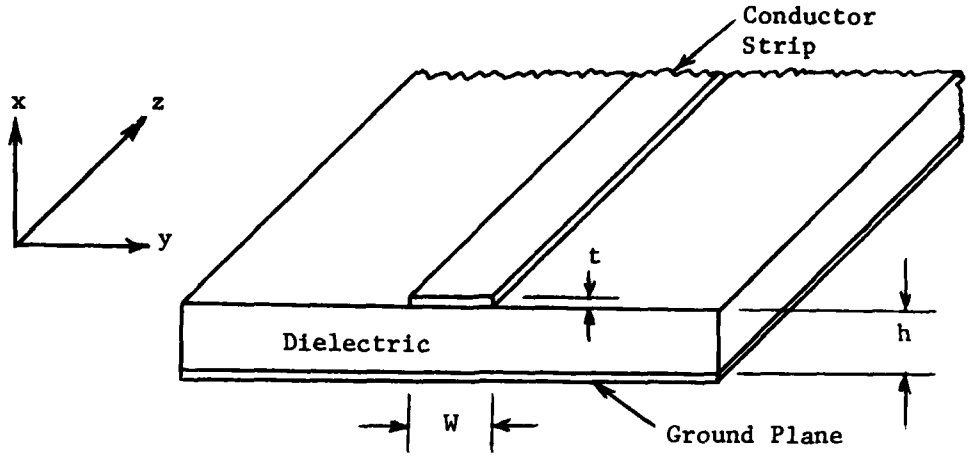

Figure 1. A Microstrip Transmission Line

The most widely used technique for analyzing microstrip structures was introduced by Wheeler[2]. His method involves the use of conformal transformation techniques for the evaluation of the capacitance with the dielectric slab removed and introduces the concept of effective dielectric constant to evaluate the capacitance when the dielectric slab is reinserted. For narrow strips ($W/h < 2$) as is the case for this study, the effective dielectric constant of the line is given by

$$\varepsilon_{re} = \frac{\varepsilon_r + 1}{2} + \frac{\varepsilon_r - 1}{2} \frac{\ln \frac{\pi}{2} + \frac{1}{\varepsilon_r} \ln \frac{4}{\pi}}{\ln \frac{8h}{W}}, \qquad (1)$$

and the characteristic impedance of the line by

$$Z_o = \frac{377}{2\pi \left(\frac{\varepsilon_r+1}{2}\right)^{\frac{1}{2}}} \left[\ln \frac{8h}{W} + \frac{1}{8} \left(\frac{W}{2h}\right)^2 - \frac{1}{2} \left(\frac{\varepsilon_r-1}{\varepsilon_r+1}\right) \left(\ln \frac{\pi}{2} + \frac{1}{\varepsilon_r} \ln \frac{4}{\pi}\right) \right], \qquad (2)$$

where ε_r is the dielectric constant of the substrate.

It follows that the wavelength on the line is

$$\lambda_g = \frac{\lambda_o}{\sqrt{\varepsilon_{re}}} = \frac{V_p}{f} \quad , \tag{3}$$

or

$$V_p = \frac{c}{\sqrt{\varepsilon_{re}}} \quad , \tag{4}$$

where λ_o is the free space wavelength, V_p is the phase velocity of the signal on the line, and c is the velocity of the signal in free space.

Dispersion is introduced by defining the dielectric constant, characteristic impedance, and effective strip width as follows[3].

$$\varepsilon_{re}(f) = \varepsilon_r - \frac{\varepsilon_r - \varepsilon_{re}}{1 + G\left(\frac{f}{f_p}\right)^2} \quad , \tag{5}$$

where $$f_p(\text{GHz}) = \frac{Z_o}{8\pi h} \quad (h \text{ in cm}) \quad , \tag{6a}$$

and $$G = 0.6 + 0.009\, Z_o \quad . \tag{6b}$$

$$Z_o(f) = \frac{377}{W_{eff}(f)\sqrt{\varepsilon_{re}(f)}} \text{ ohms} \quad , \tag{7}$$

and $$W_{eff}(f) = W + \frac{W_{eff}(0) - W}{1 - \left(\frac{f}{f_p}\right)^2} \quad , \tag{8}$$

where $W_{eff}(0)$ is obtained from Equation (7). This relationship holds for $f \ll f_p$.

In general, changes in ε_{re} and Z_o with frequency are quite small[7] and can be neglected if

$$f(\text{GHz}) \leq \frac{6}{(\varepsilon_r - 1)^{3/2}} \left(\frac{Z_o}{h}\right)^{1/2} \quad (h \text{ in mils}) \quad . \tag{9}$$

The above relationships have been extensively verified[3] over a moderate range of W/h. However, their validity for $W/h < 0.2$ as is the

case for this study, is less certain.

The losses in microstrip become quite severe as line width gets small and frequencies become high[4]. Losses contribute significantly more to pulse degradation than do dispersion effects. Of the three loss mechanisms, conductor loss or skin loss, is by far the most serious for this application. Since the substrates are alumina (Al_2O_3) with a loss tangent of approximately 2×10^{-4} at 10 GHz, the dielectric loss is very low and will contribute little to total loss[1].

The dielectric loss in dB/cm is

$$\alpha_d \simeq 27.3 \frac{q\, \varepsilon_r \tan \delta}{\varepsilon_{re}\, \lambda_\ell} \quad , \tag{10}$$

where

$$q = \frac{\varepsilon_{re} - 1}{\varepsilon_r - 1} \quad , \tag{11}$$

is the dielectric fill factor as defined by Wheeler[2] and is always less than one. The loss tangent of the material is

$$\tan \delta = \frac{\sigma}{\omega \varepsilon} \quad . \tag{12}$$

Radiation from microstrip becomes significant only when the line is in the form of an open-circuited resonator or a disk cavity resonator and has a large normalized substrate thickness ($h/\lambda_o > 0.01$) and/or the substrate has a low dielectric constant ($\varepsilon_r < 9$)[12]. For the frequency range of interest and the dimensions of the microstrip structures (i.e. $h = 35$ mils, $W = 5$ mils, and $\varepsilon_r = 9.6$) used in this study, radiation losses can be ignored providing the lines are reasonably well terminated. Radiation losses have been determined for 1/4 λ_ℓ and 1/2 λ_ℓ resonators and do become significant at high frequencies for these microwave applications[5].

For the case under study, conductor loss will be significant (see Section 3.0) and must be considered the major cause of pulse degradation. As the lines become smaller, conductor resistance will increase accordingly. The relationship of line width to conductor resistance is not easily understood because of the complex current distribution on the conductor strip. A very simple, however not very accurate, way to analyze the problem is to consider the current distribution uniformly distributed along the bottom of the strip conductor (y direction of Figure 1) and confined to one skin depth. This analogy is reasonably accurate for wide strips; however, as the strips become small other approaches are required. Assuming a uniform current distribution across the strip width, conductor loss in dB/cm can be approximated by[3]

$$\alpha_c = \frac{8.68}{Z_o W} R_s \ , \tag{13}$$

with W in cm and

$$R_s = \left(\frac{\pi f \mu_o}{\sigma}\right)^{\frac{1}{2}} \ , \tag{14}$$

where μ_o is the permeability of free space and σ is the conductivity of the conductor.

A much more accurate expression for small lines ($\frac{W}{h} \leq \frac{1}{2\pi}$) was developed by Pucel, Masse, and Hartwig[4]. A technique was utilized that expresses the skin resistance per unit length in terms of that part of the total inductance per unit length that is attributable to the skin effect, i.e., to the inductance produced by the magnetic field within the conductor. This expression is

$$\alpha_c = \frac{8.68\ R_s}{2\pi Z_o h} P\left[1 + \frac{h}{W_e} + \frac{h}{\pi W_e}\left(\ln \frac{4\pi W}{t} + \frac{t}{W}\right)\right] \text{dB/cm} \ , \tag{15}$$

with h, t, and W in cm and where

$$P = 1 - \left(\frac{W_e}{4h}\right)^2, \tag{16}$$

$$W_e = W + \Delta W, \tag{17}$$

and

$$\Delta W = \frac{t}{\pi}\left(\ln \frac{4\pi W}{t} + 1\right). \tag{18}$$

For a fixed characteristic impedance, conductor loss decreases inversely with h and increases with the square root of the frequency.

Microstrip lines will transmit higher order TE and TM modes if operation is attempted above the cutoff frequency defined by [6] as

$$f_T = \frac{c}{2\pi h}\left(\frac{2}{\varepsilon_r - 1}\right)^{\frac{1}{2}} \tan^{-1}(\varepsilon_r), \tag{19}$$

where h is in cm.

Coupling between microstrip lines must be controlled to avoid excessive crosstalk resulting in false triggering and other noise related problems. This coupling will also cause some degree of pulse degradation since energy is coupled from the primary line to the secondary line.

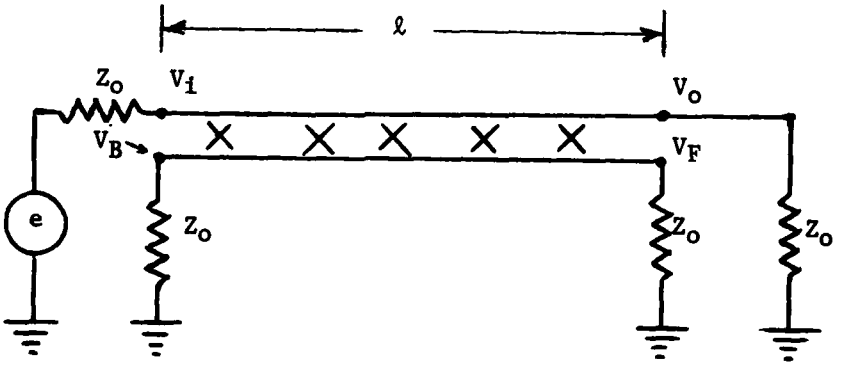

Figure 2. Coupled Lines Model

Considering the above case where both lines are terminated with the line characteristic impedance, the backward and forward induced voltages are found[8] to be

$$V_B(t) = V_2(0,t) = \frac{1}{4\sqrt{LC}}\left[Z_o C_m + \frac{L_m}{Z_o}\right]\left[V_i(t) - V_i(t-2\ell\sqrt{LC})\right], \tag{20}$$

and

$$V_F(t) = V_2(\ell,t) = \frac{\ell}{2}\left[Z_o C_m - \frac{L_m}{Z_o}\right]\frac{d}{dt} V_i(t-\ell\sqrt{LC}). \tag{21}$$

Where:

Z_o is the characteristic impedance of each line in the presence of the other;

L_m is the mutual inductance per unit length between the two lines;

C_m is the mutual capacitance per unit length between the two lines;

$V_p = \frac{c}{\sqrt{\varepsilon_{re}}} = \frac{1}{\sqrt{LC}}$;

ε_{re} is the effective dielectric constant;

and ℓ is the length of coupled section.

This assumes the lines are lossless and coupling is loose, i.e., energy induced on the secondary line is small compared to the energy on the primary line.

Defining

$$K_B = \frac{L_m}{4\, Z_o \sqrt{LC}}\left[\left(\frac{Z_o}{Z_m}\right)^2 + 1\right], \tag{22}$$

and

$$K_F = \frac{L_m}{2Z_o}\left[\left(\frac{Z_o}{Z_m}\right)^2 - 1\right], \tag{23}$$

where

$$Z_m = \left(\frac{L_m}{C_m}\right)^{1/2}, \tag{24}$$

gives

$$V_B(t) = K_B \left[V_i(t) - V_i(t - 2\ell \sqrt{LC}) \right], \tag{25}$$

and

$$V_F(t) = K_F \ell \frac{dV_i}{dt} (t - \ell \sqrt{LC}). \tag{26}$$

From these equations it is concluded that V_B (backward coupled pulse) is an attenuated replica of the driving pulse minus the signal delayed by $2\ell \sqrt{LC}$. The forward coupled pulse (V_F) varies as the first time derivative of the driving pulse delayed by $\ell\sqrt{LC}$ and is directly proportional to the coupled length. The coupling constants, K_F and K_B, can be determined experimentally from the following relationships if the signal rise-time is less than 2 times the propagation delay of the coupled section.

$$K_B = \frac{V_B}{V_o}, \tag{27}$$

and

$$K_F = \frac{V_{Fmax}}{\left.\frac{dV_o}{dt}\right|_{max}} \frac{1}{\ell} \left(\frac{\text{time}}{\text{unit length}}\right). \tag{28}$$

3.0 SAMPLE MICROSTRIP CALCULATIONS

From the following calculations, the approximate results to be anticipated from measurements are determined as is the significance of considering dispersion effects.

The design criteria used are as follows:

W (line width) = 5 mils

t (line thickness) = 1 mil

h (substrate thickness) = 35 mils

ε_r (relative dielectric constant of alumina) = 9.6

From Equation (1), it is found that

$$\varepsilon_{re} = 5.8 \ .$$

From Equation (2), it is found that

$$Z_o = 100 \text{ ohms} \ .$$

From Equation (9), it is found that

$$f \leq 5.9 \text{ GHz} \ .$$

From Equation (7) with f = 0

$$W_{eff}(0) = 54.79 \text{ mils} \ .$$

From Equation (5), (6a), and (6b), it is found that

$$G = 1.5 \ ,$$

$$f_p = 44.76 \text{ GHz} \ ,$$

and

$$\varepsilon_{re}(0) = 5.8 \ ,$$

$$\varepsilon_{re}(10 \text{ GHz}) = 6.06 \ ,$$

$$\varepsilon_{re}(20 \text{ GHz}) = 6.68 \ .$$

The change in ε_{re} from DC to 20 GHz is 15%. The change in ε_{re} from DC to 10 GHz is 4.5%.

From Equation (8), it is found that

$$W_{eff}(0) = 54.79 \text{ mils} ,$$

$$W_{eff}(10 \text{ GHz}) = 52.39 \text{ mils} ,$$

$$W_{eff}(20 \text{ GHz}) = 46.51 \text{ mils} .$$

The change in W_{eff} from DC to 20 GHz is 15%. The change in W_{eff} from DC to 10 GHz is 4.5%.

From Equation (7), it is found that

$$Z_o(0) = 100 \text{ ohms} ,$$

$$Z_o(10 \text{ GHz}) = 102 \text{ ohms} ,$$

$$Z_o(20 \text{ GHz}) = 110 \text{ ohms} .$$

The change in Z_o between DC and 20 GHz is 10%. The change in Z_o between DC and 10 GHz is 2%.

From Equation (4), it is found that

$$V_p(0) = 1.25 \times 10^{10} \text{ cm/sec} ,$$

$$V_p(10 \text{ GHz}) = 1.22 \times 10^{10} \text{ cm/sec} ,$$

$$V_p(20 \text{ GHz}) = 1.16 \times 10^{10} \text{ cm/sec} .$$

The change in V_p between DC and 20 GHz is 7.2%. The change in V_p between DC and 10 GHz is 2.4%.

From Equation (10), (3), and (11); and, using $\tan \delta$ (10 GHz) = 2×10^{-4}

$$\alpha_d(10 \text{ GHz}) = 4 \times 10^{-3} \text{ dB/cm} .$$

From Equation (15), (16), (17), and (18); and using the thick film ink manufacturer's data for surface resistivity, R_s = 0.002 ohm/square ($1/\sigma$ = 5.08×10^{-8} ohm meters),

$$\alpha_c = 9.47 \times 10^{-7} \sqrt{f} \text{ dB/cm} ;$$

thus,

$$\alpha_c(1 \text{ GHz}) = 0.030 \text{ dB/cm} ,$$

$$\alpha_c(5\ \text{GHz}) = 0.067\ \text{dB/cm}\ ,$$

$$\alpha_c(10\ \text{GHz}) = 0.095\ \text{dB/cm}\ ,$$

$$\alpha_c(20\ \text{GHz}) = 0.134\ \text{dB/cm}\ .$$

Since $R_{DC} = R_S \times S$,

where S is the number of squares

$$R_{DC} = 0.157\ \text{ohms/cm}\ .$$

Using a load resistance of 50 ohms,

$$\alpha_c(0) = 2.64 \times 10^{-2}\ \text{dB/cm}\ .$$

In summary, over the frequency range from DC to 10.0 GHz changes in the characteristic impedance and the phase velocity are limited to 2.5%. For all practical purposes this can be ignored. Over the frequency range DC to 20.0 GHz changes in characteristic impedance and phase velocity are limited to 10%. These changes will result in some dispersion. However, as will be shown in Section 6.0 the frequency components in the 10.0 to 20.0 GHz range for the pulses of interest are very small and thus changes in phase velocity will not degrade the integrity of these pulses to any noticeable extent.

Dielectric loss will be very small and can be considered insignificant when compared to conductor loss. The conductor loss is a strong function of frequency and will be the major contributing factor to pulse degradation.

4.0 EXPERIMENTAL APPROACH TO DEVELOPING THE TRANSFER CHARACTERISTICS OF MICROSTRIP LINES USING FAST RISETIME STEP FUNCTIONS

The interconnect lines between high speed digital logic devices must be designed to preserve the integrity of the pulses to the maximum extent possible. Since conflicting design requirements will often result in non-optimum design in terms of any one of several parameters, the extent of pulse degradation due to non-optimum electrical design must be understood in order to make objective trade-offs.

The transmission line is considered as a linear system with transfer function $H(\omega)$.

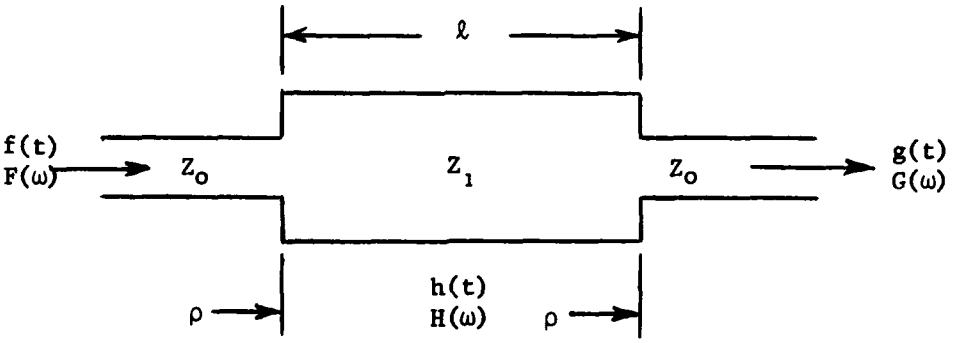

Figure 3. Transmission Line Model

$H(\omega)$ is of the general form $A(\omega)e^{j\theta(\omega)}$ where $A(\omega)$ is the amplitude function and $\theta(\omega)$ is the phase function. Denoting

$$f(t) \leftrightarrow F(\omega),$$

$$g(t) \leftrightarrow G(\omega),$$

$$h(t) \leftrightarrow H(\omega),$$

as Fourier transform pairs then

$$g(t) = f(t) * h(t), \tag{29}$$

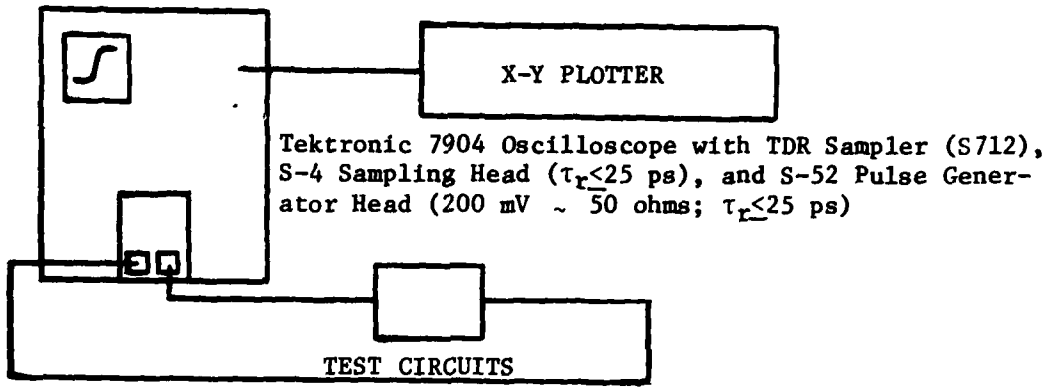

Figure 4. Test Circuit for Measuring Attenuation, Pulse Risetime, and Coupling Parameters.

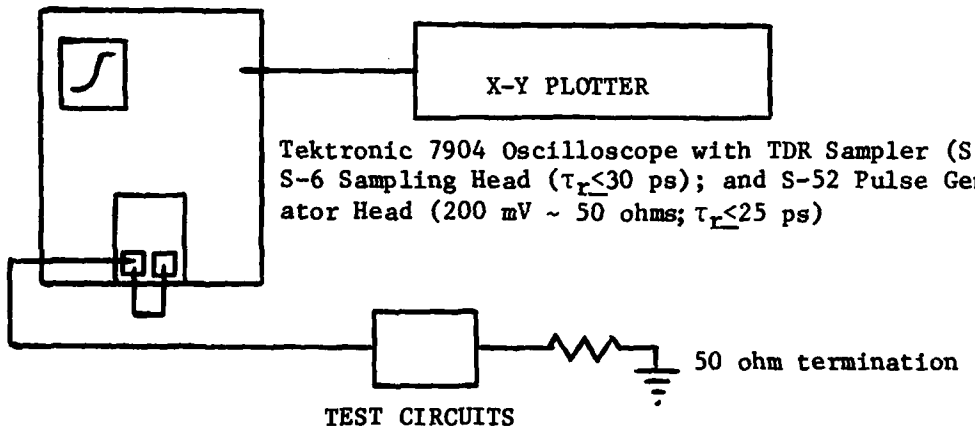

Figure 5. Test Circuit for Measuring Characteristic Impedance, Signal Propagation Velocity, and Reflection Coefficients.

$$G(\omega) = F(\omega)\ H(\omega), \tag{30}$$

and

$$H(\omega) = \frac{G(\omega)}{F(\omega)} = A(\omega)\ e^{j\theta(\omega)}. \tag{31}$$

From the sample calculations for a 5 mil gold line on 35 mil alumina, the dispersion effects are minimal, therefore, $\theta(\omega)$ can for all practical purposes be considered linear ($\theta(\omega) = -t_o\omega$). This being the case, if f(t) has even symmetry about t=0, g(t) will have even symmetry about $t=t_o$, where t_o is the time delay. Since the equipment that was used to characterize the transmission lines (see Figures 4 and 5) generated a step function and not a complete pulse, a mirror image of the step function was artificially generated. The Fourier series coefficients could then be calculated (see Figure 6).

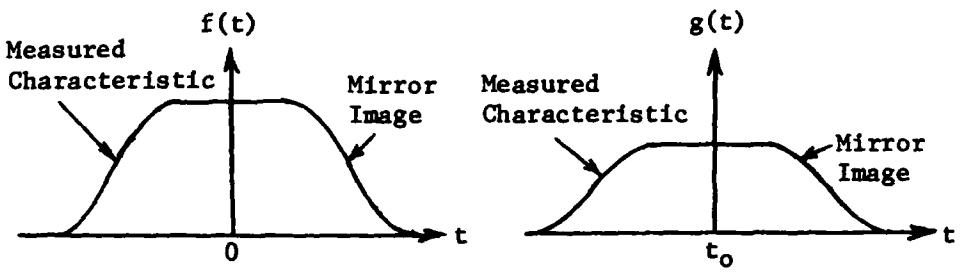

Figure 6. Input and Output Pulses Constructed From Step Functions

Using this approach the Fourier coefficients of f(t) and g(t) were calculated using the HP 9820 calculator routine "Fourier Series Coefficients for Unequally Spaced Data Points" with

$$f(t) = a_o + \sum_{n=1}^{\infty} a_n \cos n\omega_o t + b_n \sin n\omega_o t, \tag{32}$$

then

$$a_o = \frac{1}{T} \int_{-\frac{T}{2}}^{\frac{T}{2}} f(t)\, dt, \tag{33}$$

$$a_n = \frac{2}{T} \int_{-\frac{T}{2}}^{\frac{T}{2}} f(t) \cos n\omega_o t\, dt \qquad n = 1,2,3,\ldots, \tag{34}$$

$$b_n = \frac{2}{T} \int_{-\frac{T}{2}}^{\frac{T}{2}} f(t) \sin n\omega_o t\, dt \qquad n = 1,2,3,\ldots, \tag{35}$$

with

$$\omega_o = \frac{2\pi}{T} . \tag{36}$$

Since f(t) has even symmetry, all the b_n coefficients go to zero thus a cosine series remains.

In order to analyze the pulses and transform characteristics in terms of meaningful parameters, an idealized trapezoidal pulse was also studied.

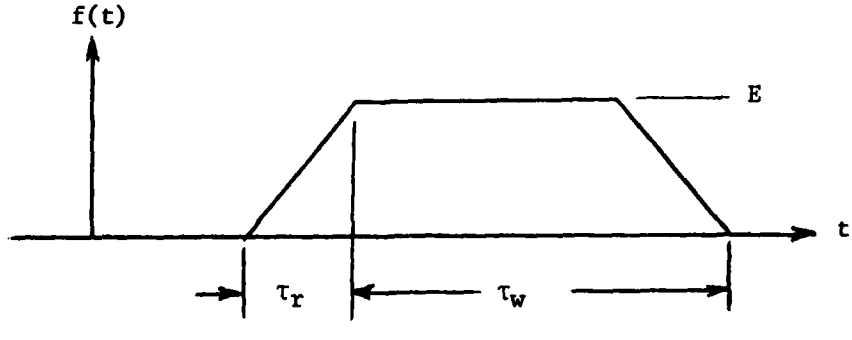

Figure 7. Idealized Trapezoidal Pulse

Consider the idealized trapezoidal pulse of Figure 7 with a Fourier transform

$$F(\omega) = E\tau_w \frac{\sin \omega(\frac{\tau_r}{2})}{\omega(\frac{\tau_r}{2})} \frac{\sin \omega(\frac{\tau_w}{2})}{\omega(\frac{\tau_w}{2})} . \tag{37}$$

As $\tau_r \to 0$ the well defined spectrum of a rectangular pulse emerges.

$$F(\omega) = E\tau_w \frac{\sin \omega \frac{\tau_w}{2}}{\omega(\frac{\tau_w}{2})} . \tag{38}$$

As $\tau_w \to \tau_r$ the well defined spectrum of an isosceles triangular pulse emerges.

$$F(\omega) = E\tau_r \frac{\sin^2 \omega(\frac{\tau_r}{2})}{\omega(\frac{\tau_r}{2})^2} . \tag{39}$$

Since the actual pulse of interest is not an idealized trapezoid, the Fourier transform of the idealized pulse is modified by a degradation factor $Y(\omega)$.

$$F(\omega) = E\tau_w \frac{\sin \omega(\frac{\tau_r}{2})}{\omega(\frac{\tau_r}{2})} \frac{\sin \omega(\frac{\tau_w}{2})}{\omega(\frac{\tau_w}{2})} Y(\omega). \tag{40}$$

Defining

$$X(\omega) = \frac{\sin \omega (\frac{\tau_r}{2})}{\omega(\frac{\tau_r}{2})} Y(\omega), \tag{41}$$

gives

$$F(\omega) = E\tau_w \frac{\sin \omega(\frac{\tau_w}{2})}{\omega(\frac{\tau_w}{2})} X(\omega). \tag{42}$$

Converting to a discrete transform,

$$F(n\omega_o) = E\tau_w \frac{\sin n\omega_o(\frac{\tau_w}{2})}{n\omega_o(\frac{\tau_w}{2})} X(n\omega_o). \tag{43}$$

In terms of the previously defined coefficients for the single ended spectrum,

$$a_n = \frac{F(n\omega_o)}{T} = \frac{E\tau_w}{T} \frac{\sin n\omega_o (\frac{\tau_w}{2})}{n\omega_o(\frac{\tau_w}{2})} X(n\omega_o). \tag{44}$$

Assuming that $X(\omega)$ has the general form of a low pass filter with a cut-off frequency much greater than $\frac{1}{\tau_w}$, τ_w can be defined from the first zero crossing of $F(\omega)$,

i.e., setting $\sin \omega(\frac{\tau_w}{2}) = 0,$

by making $\omega(\frac{\tau_w}{2}) = \pi,$

gives $\tau_w = \frac{1}{f}.$ (45)

Now that the pulse width (τ_w) is defined, the pulse amplitude (E) is calculated using

$$E = \frac{a_o T}{\tau_w}. \tag{46}$$

The remaining pulse parameter to be defined is the pulse risetime (τ_r). If one could determine from the frequency spectrum the frequency at which $\sin \omega(\frac{\tau_r}{2})$ equals zero, τ_r could be easily calculated. However, the high frequency components are very small and the effect $Y(\omega)$ has on the pulse make it impossible to identify this point from the spectrum. A second approach would be to use the time it takes to go from 10% to 90% of the pulse peak amplitude. However, this conventional approach can be misleading if the pulse has much overshoot. From the idealized trapezoidal pulse the risetime is defined in terms of the derivative of f(t) at the previously defined pulse width point.

$$\tau_r \triangleq \frac{E}{\left.\frac{df(t)}{dt}\right|_{\tau_w}} \quad . \tag{47}$$

Using Equation 44 with calculated values of a_n and τ_w, the first eleven terms of $X(n\omega_o)$ were calculated for both the input (f(t)) and output (g(t)) pulses. A pulse period of 4 ns was used (f_o = 250 MHz). Additional terms could be calculated but the accuracy degrades as the values of a_n become small.

Recognizing that the $X(n\omega_o)$ terms are normalized by the pulse amplitude, pulse width, and pulse width function; the discrete transfer function becomes

$$A(n\omega_o) = k \frac{X(n\omega_o)_{out}}{X(n\omega_o)_{in}} \quad , \tag{48}$$

where

$$k = \frac{E_{out}}{E_{in}} \quad , \tag{49}$$

with E_{out} and E_{in} defined by Equation 45. The pulse width (τ_w) is ignored since it was arbitrarily selected and normalized out of the equations.

It was felt the transfer function could best be described in terms of a polynomial, $P(x) = b_0 + b_1x^1 + b_2x^2 + \ldots + b_nx^n$. A curve fitting routine that uses Chebyshev polynomials was thus used to calculate the b_n coefficients from the experimental and theoretical values of $A(n\omega_o)/k$. This approach assumes the values of $A(n\omega_o)/k$ are independent random variables having normal distribution with common variance. By proper selection of degree (number of b_n terms calculated) the curve can be chosen that best fits the points and also allows extrapolation to higher

frequencies. Pulse risetimes defined by Equation 47 were also compared to the time it takes the pulse to go from 10% to 90% of the peak amplitude and to the time defined by Equation 47, only using the maximum risetime rate instead of risetime rate at the pulse width point defined by Equation 45.

5.0 DESCRIPTION OF THE TEST CIRCUITS

The term thick film has gained acceptance as the preferred generic description for that field of microelectronics in which specifically formulated pastes are applied and fired onto a ceramic substrate in a definite pattern and sequence to produce either a set of individual components such as resistors and capacitors or a complete functional circuit. The pastes are usually applied using a silk-screen method. The high temperature firing matures the thick film elements and bonds them integrally to the ceramic substrate[10].

The test circuits were fabricated in this way using ESL 8835-1B gold paste on 99.6% pure alumina (Al_2O_3). Five (5) mil lines were screened onto the 4 inch by 5 inch by 35 mil thick substrates using a 325 mesh stainless steel screen. The test substrates were then mounted on a specially designed test fixture (see Figure 10) that interfaced the microstrip lines to OSM type coaxial output connectors. The microstrip lines were transformed from 50 ohm characteristic impedance to 100 ohm characteristic impedance using a 1/2 inch linear taper.

Right angle line bends (see line No. 2, Figure 8) were evaluated using Time Domain Reflectometer (TDR) techniques. Three line lengths, three coupling lengths, and three coupling line separations were evaluated. All lines were approximately 5 mils wide and 1 mil thick. It was determined that smaller lines could not be deposited reliably using thick film fabrication techniques and that lines spaced closer than 5 mils would short together, particularly for long coupling lengths (> 1.0 inches). It should also be noted that the width (W) along the lines varied up to 0.5 mils. This is the result of inherent limitations in

the fabrication process. It was however judged that this variation would not have a significant adverse impact on the test results.

Line lengths of 10.16 cm, 21.27 cm, and 30.48 cm were evaluated. Coupled line lengths of 2.54 cm, 5.08 cm, and 7.62 cm were evaluated as were line separations of 5 mils, 10 mils, and 15 mils (see Figures 8 and 9). Test equipment used is shown in Figures 4 and 5. Pulse rise-time was varied by changing cable lengths.

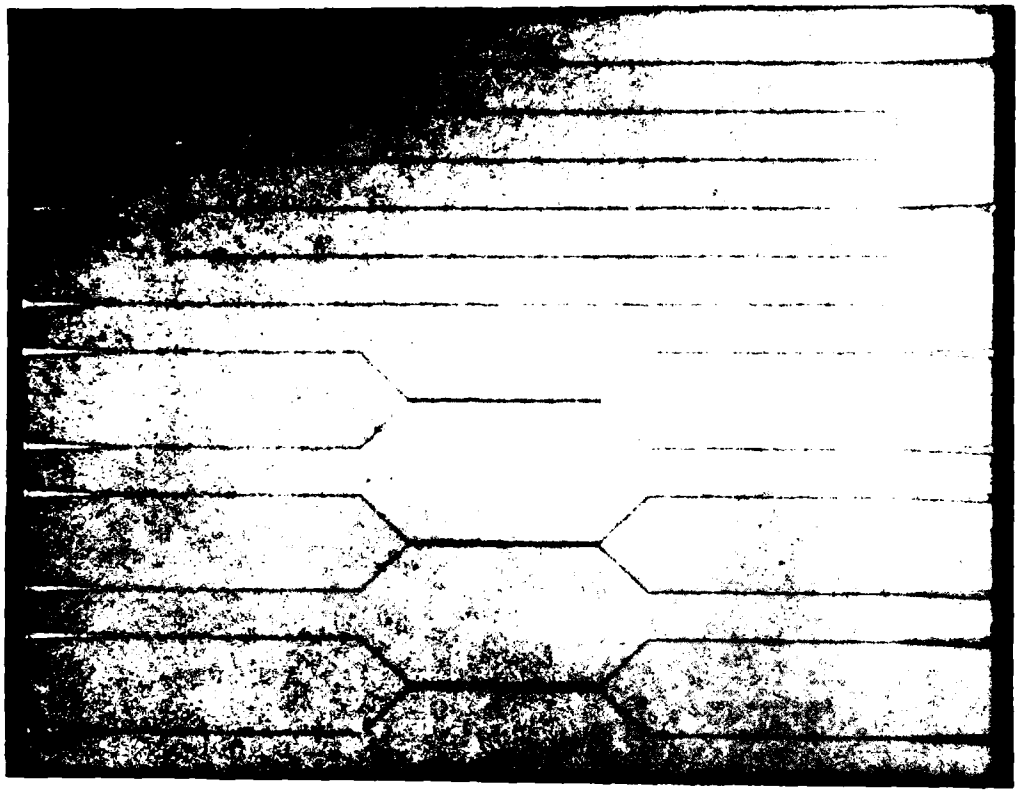

Figure 8. Test Circuit No. 1. Alumina Substrate is 4 inches by 5 inches by 35 mils Thick. Microstrip Lines are 5 mils Wide.

Figure 9. Test Circuit No. 2. Alumina Substrate is 4 inches by 5 inches by 35 mils Thick. Microstrip Lines are 5 mils Wide.

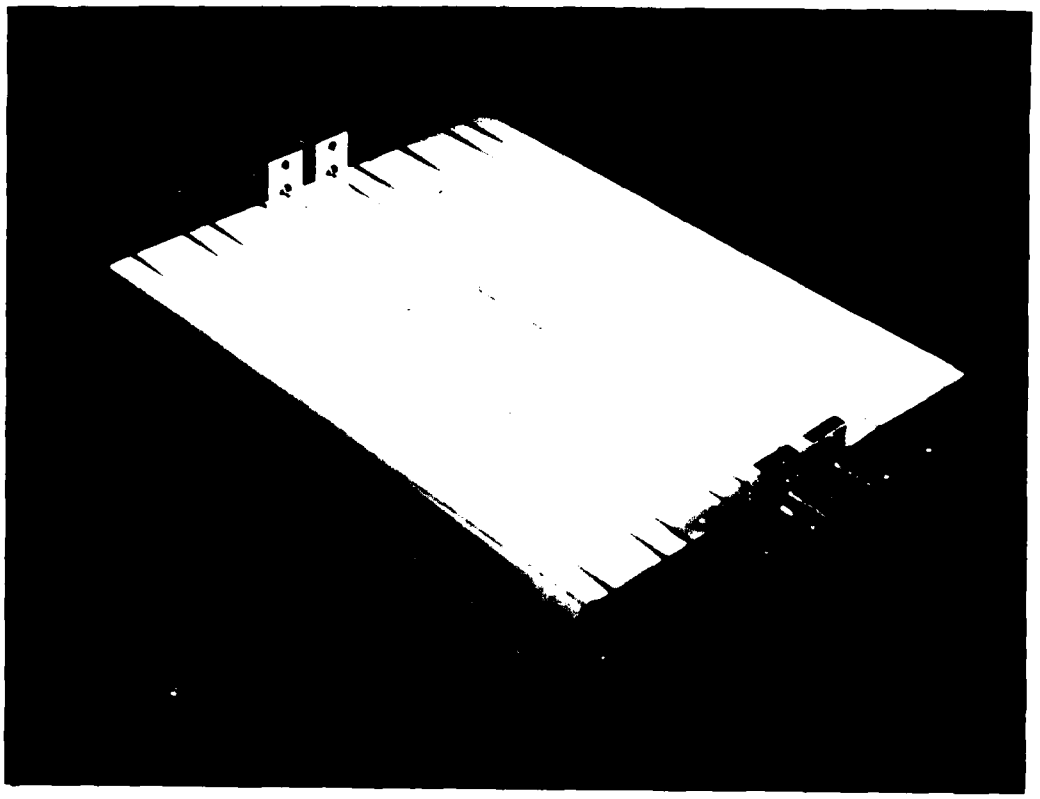

Figure 10. Test Circuit with Microstrip to Coaxial Transitions

6.0 TEST RESULTS

6.1 Characteristic Impedance:

Using the test setup of Figure 5, the line characteristic impedance is calculated as[11],

$$Z_1 = Z_o \frac{1+\rho}{1-\rho} \quad , \tag{50}$$

$$Z_1 = 104 \text{ ohms} \quad ,$$

where the characteristic impedance of the test system (Z_o) is 50 ohms and ρ is the reflection coefficient from Figure 11.

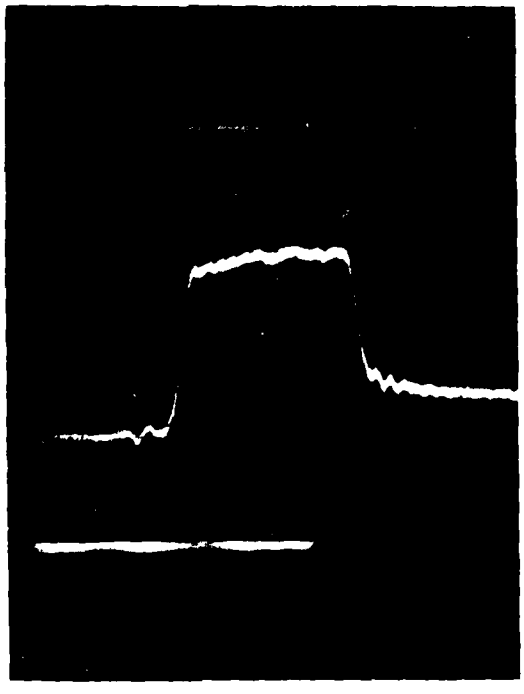

Figure 11. Time Domain Reflectometer (TDR) Display from Line 1, Figure 8, Showing the Line Characteristic Impedance and the Propagation Delay. Line Width is 5 mils. Line Length is 10.16 cm and the Pulse Risetime is 70 ps. Vertical = 0.02 ρ/div.; Horizontal = 0.5 ns/div.

6.2 Propagation Velocity:

$$V_p = \frac{\ell}{T_D} \quad , \tag{51}$$

$$V_p = 1.27 \times 10^8 \text{ m/sec},$$

where $2T_d = 1.6 \times 10^{-9}$ sec from Figure 11 and $\ell = 10.16$ cm (Line No. 1, Figure 8).

6.3 Effective Dielectric Constant:

$$V_p = \frac{c}{\sqrt{\varepsilon_{re}}} \quad \text{(Equation (4))} \ ,$$

$$\varepsilon_{re} = 5.58 \ .$$

6.4 Reflection Coefficient:

The reflection coefficient caused by the two 90^o bends separated by 0.635 cm (Line No. 2, Figure 8) is calculated as [11],

$$Z_2 = Z_1 \left[\frac{200 \ Z_1 + \rho_2 \ (Z_1 + 50)^2}{200 \ Z_1 - \rho_2 \ (Z_1 + 50)^2} \right] \ , \tag{52}$$

using $Z_1 = 106.25$ ohms and $\rho_2 = -0.05$ from Figure 12,

$$Z_2 = 94.7 \text{ ohms}.$$

To calculate the reflection coefficient relative to the line characteristic impedance (Z_1),

$$\rho = \frac{Z_2 - Z_1}{Z_2 + Z_1} \ , \tag{53}$$

$$\rho = -0.06 \ .$$

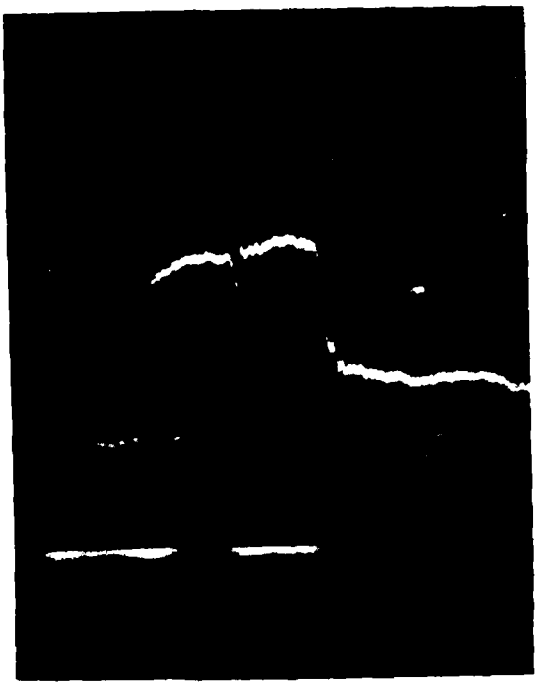

Figure 12. Time Domain Reflectometer (TDR) Display from Line 2, Figure 8, Showing the Reflection Coefficient Caused by Two 90° Bends Separated by 0.635 cm. Line Width is 5 mils. Pulse Risetime is 70 ps. Vertical = 0.02 ρ/div.; Horizontal = 1 ns/div.

6.5 Characteristic Impedance of Coupled Lines:

Using the same technique as in Section 6.4, the characteristic impedance (Z_2) of the coupled line segments and the resulting reflection coefficients (ρ) are calculated for Line Pairs 4, 5, and 6 of Figure 8. Results are:

For Line Pair No. 4 (line spacing is 5 mils), and from Figure 13,

$$\rho_2 = -0.04 ,$$
$$Z_2 = 96.9 \text{ ohms}$$

and $\rho = -0.05$.

For Line Pair No. 5 (line spacing is 10 mils), and from Figure 14,

$$\rho_2 = -0.03 ,$$

$$Z_2 = 99.2 \text{ ohms} ,$$

and $\rho = -0.03$.

For Line Pair No. 6 (line spacing is 15 mils), and from Figure 15,

$$\rho_2 = -0.01 ,$$

$$Z_2 = 103.8 \text{ ohms} ,$$

and $\rho = -0.01$.

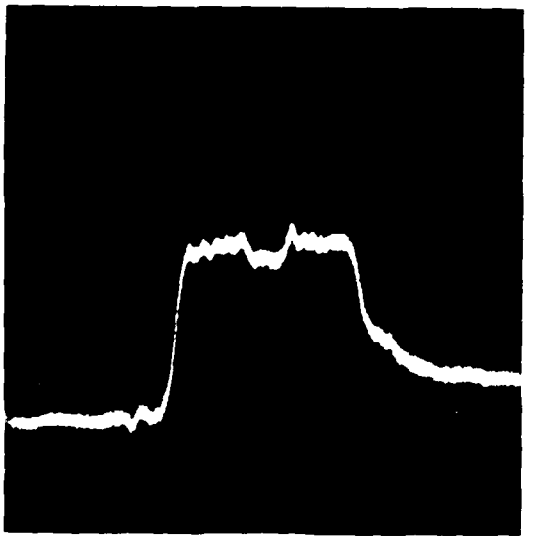

Figure 13. Time Domain Reflectometer (TDR) Display from Line Pair No. 4, Figure 8, Showing the Characteristic Impedance (Z_2) of the Coupled Section. Line Width is 5 mils. Line Spacing is 5 mils. Vertical = 0.02 ρ/div.; Horizontal = 0.5 ns/div.

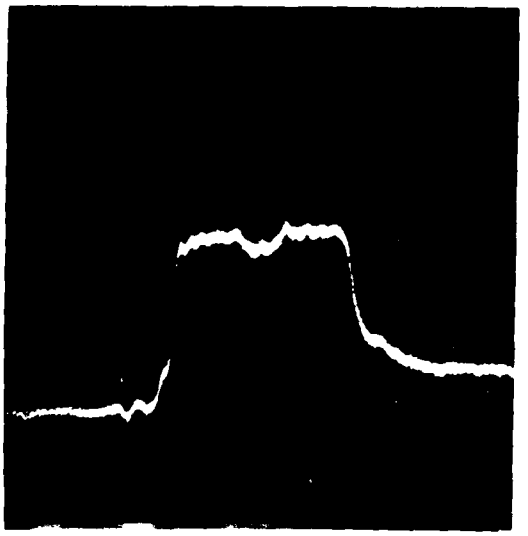

Figure 14. Time Domain Reflectometer (TDR) Display from Line Pair No. 5, Figure 8, Showing the Characteristic Impedance (Z_2) of the Coupled Section. Line Width is 5 mils. Line Spacing is 10 mils. Vertical = 0.02 ρ/div.; Horizontal = 0.5 ns/div.

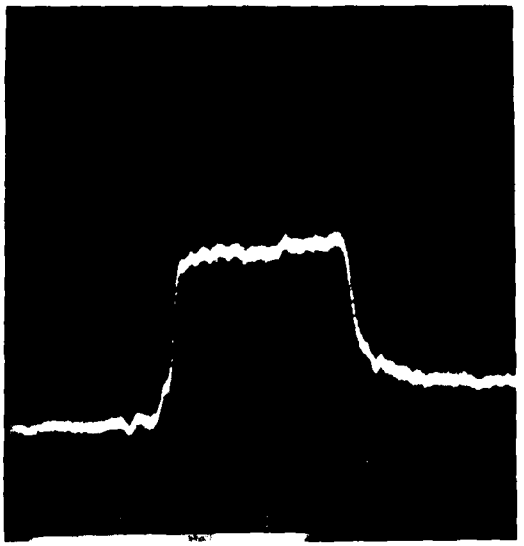

Figure 15. Time Domain Reflectometer (TDR) Display from Line Pair No. 6, Figure 8, Showing the Characteristic Impedance (Z_2) of the Coupled Section. Line Width is 5 mils. Line Spacing is 15 mils. Vertical = 0.02 ρ/div.; Horizontal = 0.5 ns/div.

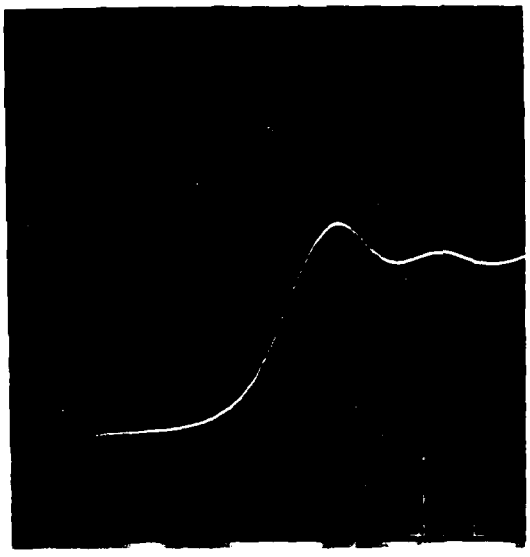

Figure 16. Output Step Function (V_o) from Line Pair No. 5, Figure 8, with Coupled Line Terminated with 50 ohms. (s = 10 mils, W = 5 mils, ℓ = 2.54 cm). Vertical = 50 mV/div.; Horizontal = 50 ps/div.

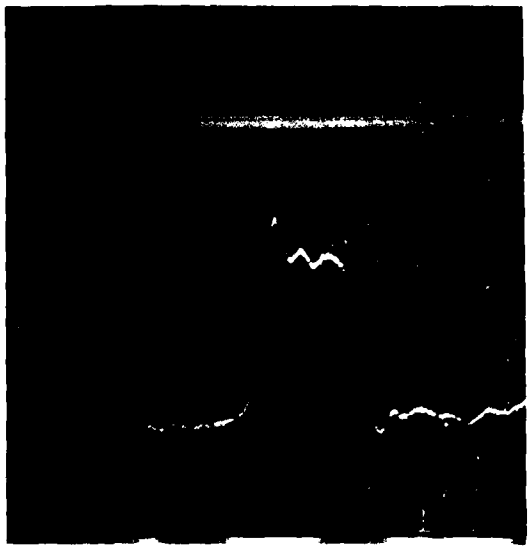

Figure 17. Reverse Coupled Signal from Line Pair No. 5, Figure 8 (s = 10 mils, ℓ = 2.54 cm). All Lines are Terminated with 50 ohms. Line Width is 5 mils. Vertical = 0.20 mV/div.; Horizontal = 200 ps/div.

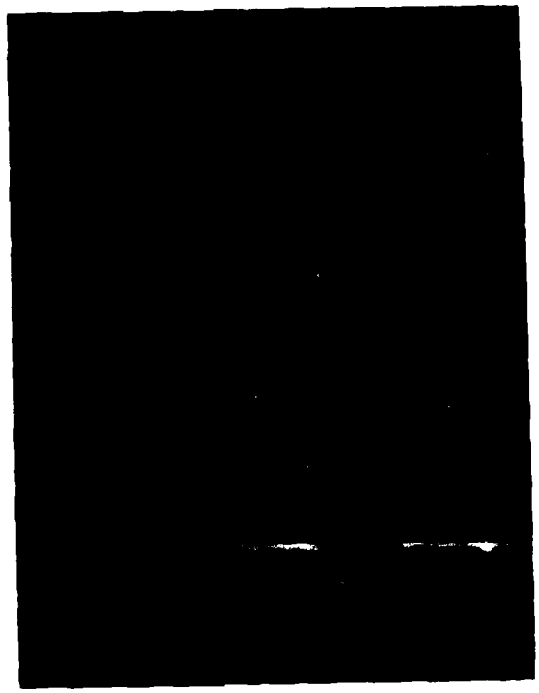

Figure 18. Forward Coupled Signal from Line Pair No. 5, Figure 8 (s = 10 mils, ℓ = 2.54 cm). All Lines are Terminated with 50 ohms. Line Width is 5 mils. Vertical = 5 mV/div.; Horizontal = 50 ps/div.

6.6 Coupling Characteristics as a Function of Maximum Signal Risetime Rate:

Using the test setup of Figure 4, the coupled signals were measured as a function of output signal (V_o) risetime rate. Figure 19 shows the results. The reverse coupled signal, normalized to the output signal (V_o) amplitude, is independent of maximum signal risetime rate while the forward coupled signal, also normalized to the output signal amplitude, decreases slightly with increased risetime rate. Line Pair

No. 5 (s = 10 mils; ℓ = 2.54 cm) of Figure 8 was used to obtain these data.

From Equations (27) and (28), the Forward (K_F) and Backward (K_B) coupling coefficients were calculated and plotted in Figures 20 and 21 as functions of the maximum output signal risetime rate. The coupling coefficients are relatively unaffected by changes in risetime.

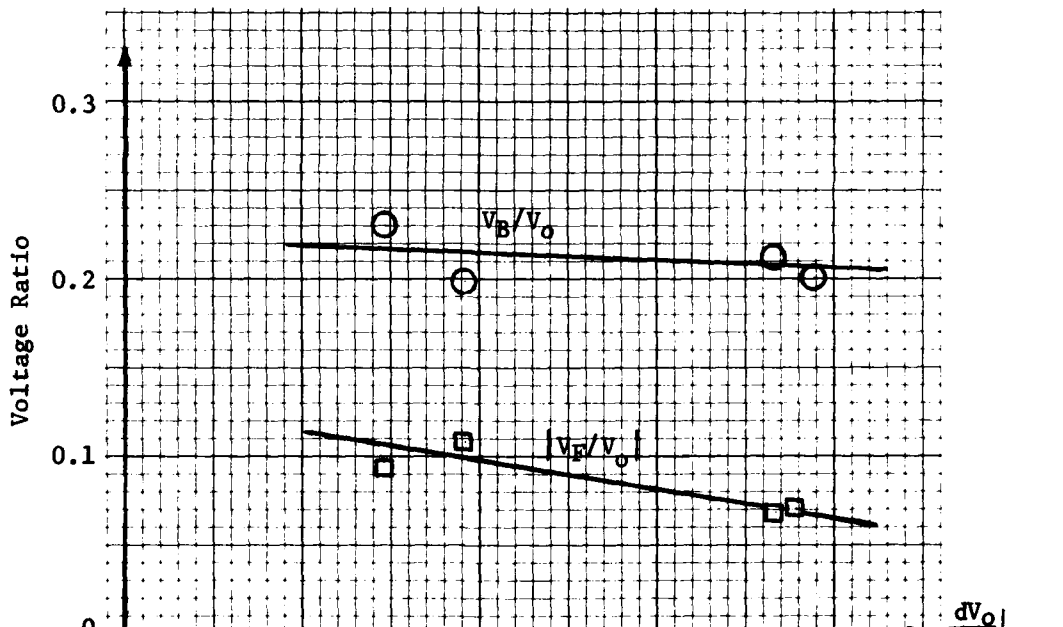

Figure 19. Forward (V_F) and Backward (V_B) Coupled Voltages Normalized to the Output Voltage (V_o) as a Function of Maximum Output Signal Risetime Rate in mV/ps. Line Pair No. 5, Figure 8 (s = 10 mils, ℓ = 2.54 cm, and w = 5 mils) was Used to Obtain These Data.

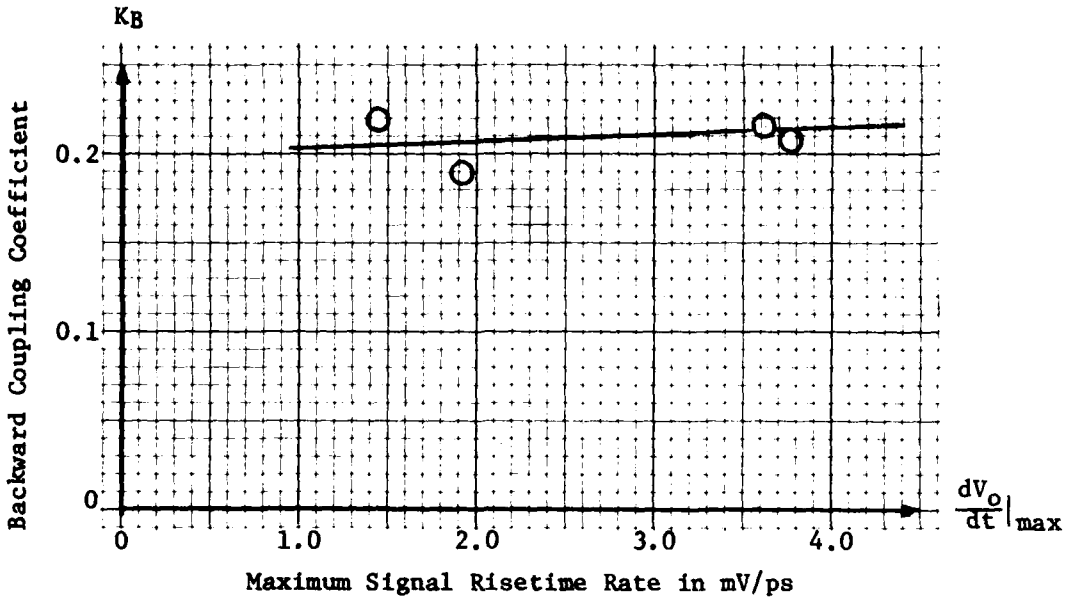

Figure 20. Backward Coupling Coefficients (K_B) as a Function of Maximum Output Signal (V_o) Risetime Rate in mV/ps. Line Pair No. 5, Figure 8 (s = 10 mils, ℓ = 2.54 cm, and W = 5 mils) was Used to Obtain These Data.

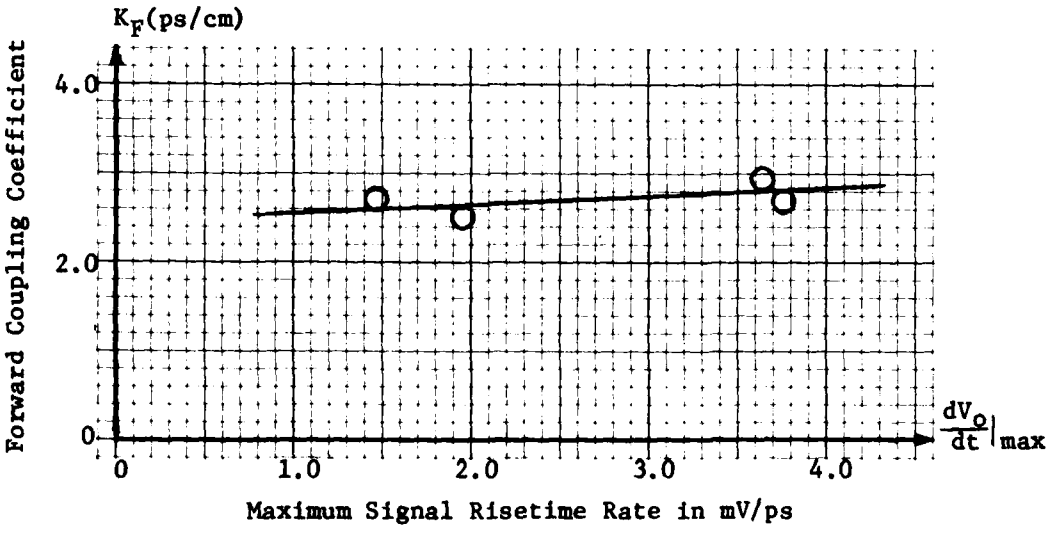

Figure 21. Forward Coupling Coefficients (K_F) as a Function of Maximum Output Signal (V_o) Risetime Rate in mV/ps. Line Pair No. 5, Figure 8 (s = 10 mils, ℓ = 2.54 cm, and W = 5 mils) was Used to Obtain These Data.

6.7 Coupling Characteristics as a Function of Coupled Line Length:

Using the test setup of Figure 4, the effects of coupled line length on coupled signal amplitude were measured. From Figure 22, the backward coupled signal is practically unaffected by coupling length while the forward coupled signal is directly proportional to coupled length.

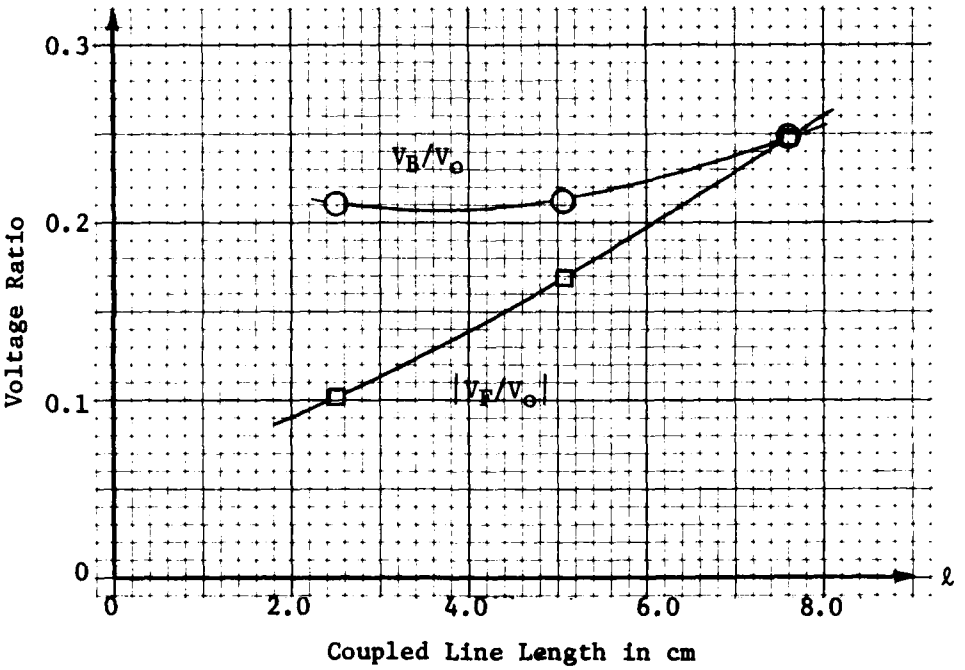

Figure 22. Forward (V_F) and Backward (V_B) Coupled Voltages Normalized to the Output Voltage (V_o) as a Function of Coupled Line Length in cm. Line Spacing is 10 mils. Maximum Output Signal Risetime Rate is 3.68 mV/ps.

Forward (K_F) and Backward (K_B) coupling coefficients were calculated and plotted as functions of coupled line length in Figures 23 and 24. The backward coupling coefficients increase slightly with coupled line length while the forward coupling coefficient decreases slightly.

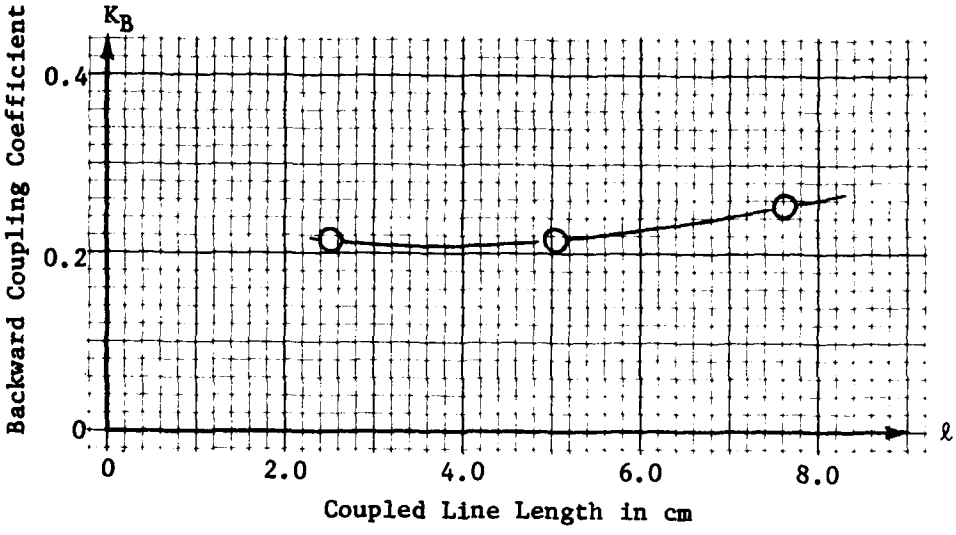

Figure 23. Backward Coupling Coefficients (K_B) as a Function of Coupled Line Length for a Line Spacing of 10 mils. Maximum Output Signal Risetime Rate is 3.68 mV/ps.

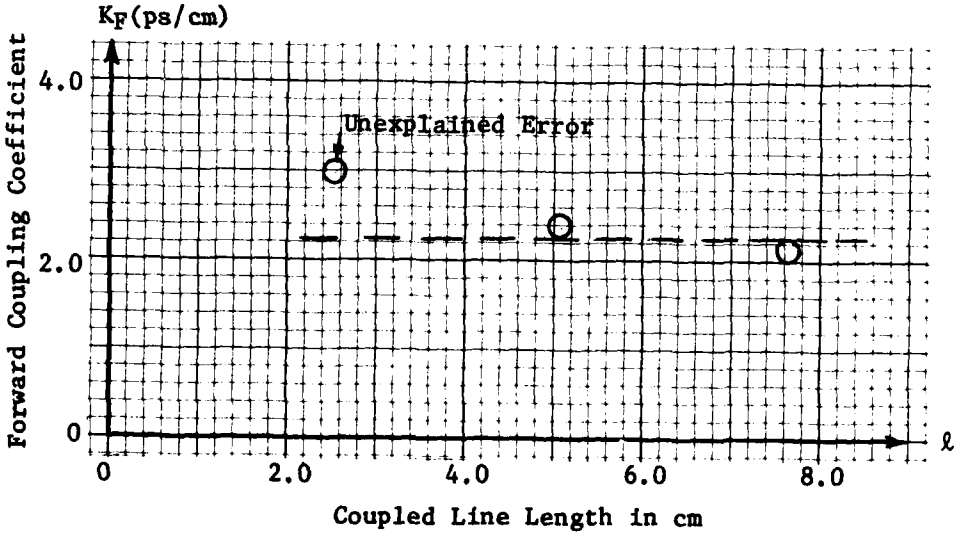

Figure 24. Forward Coupling Coefficients (K_F) as a Function of Coupled Line Length for a Line Spacing of 10 mils. Maximum Output Signal Risetime Rate is 3.68 mV/ps.

6.8 Coupling Characteristics as a Function of Line Spacing:

The forward and backward coupled signals were measured as functions of line spacing using the test setup of Figure 4. Line Pairs 4, 5, and 6 of Figure 8 were used where the coupled length (ℓ) is 2.54 cm. As shown in Figure 25, the backward coupled signal amplitude is a strong function of line spacing while the forward coupled signal maximizes around s = 10 mils and decreases considerably as s either increases or decreases.

The coupling coefficients as defined by Equations (27) and (28) are plotted in Figures 26 and 27. As would be expected, the coupling is significantly influenced by line spacing.

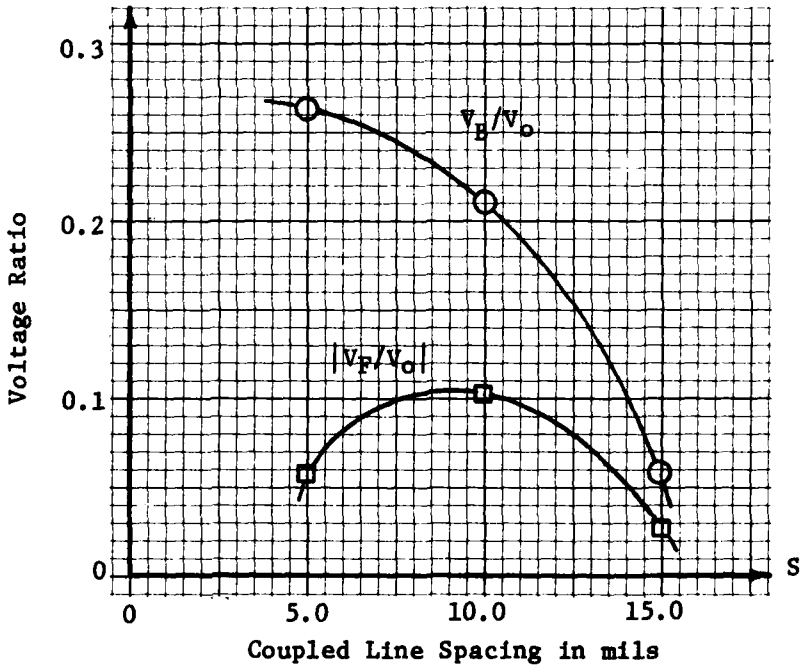

Figure 25. Forward (K_F) and Backward (K_B) Coupled Voltages Normalized to the Output Voltage (V_o) as a Function of Coupled Line Spacing. Coupled Line Length is 2.54 cm. Maximum Output Signal Risetime Rate is 3.68 mV/ps.

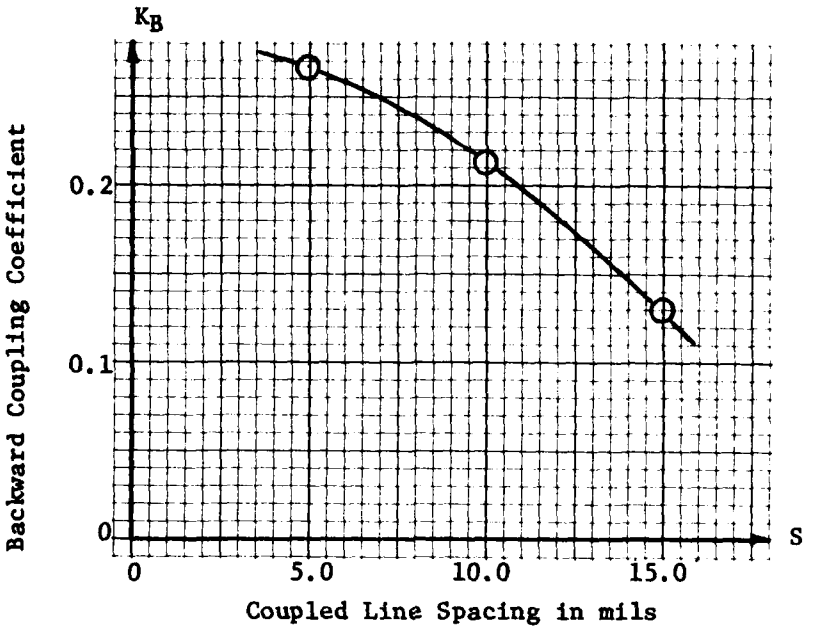

Figure 26. Backward Coupling Coefficients (K_B) as a Function of Coupled Line Spacing for a Line Length of 2.54 cm. Maximum Output Signal Risetime Rate is 3.68 mV/ps.

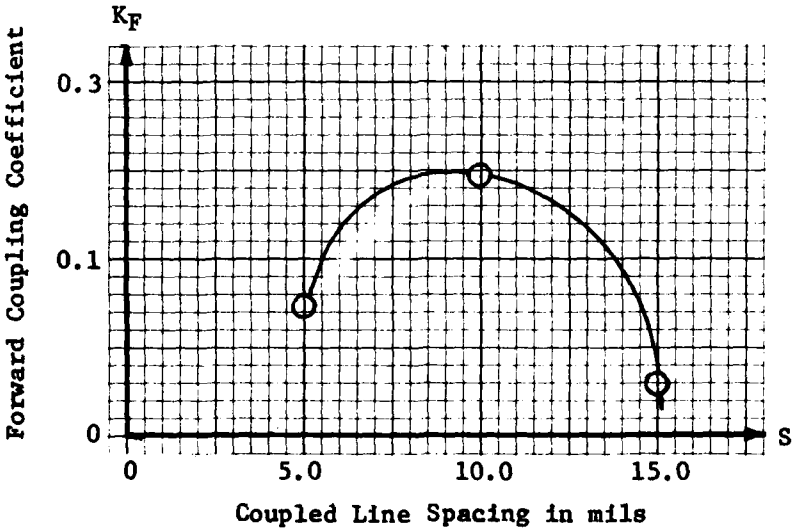

Figure 27. Forward Coupling Coefficients (K_F) as a Function of Coupled Line Spacing for a Line Length of 2.54 cm. Maximum Output Signal Risetime Rate is 3.68 mV/ps.

6.9 Risetime Degradation with Line Length:

Using the test setup of Figure 4 and Lines 1, 2, and 3 of Figure 8; the signal risetime degradation as a function of line length was determined. This data is plotted in Figure 28. Input signal risetime was varied by changing the length of the coaxial cable leading to the test fixture.

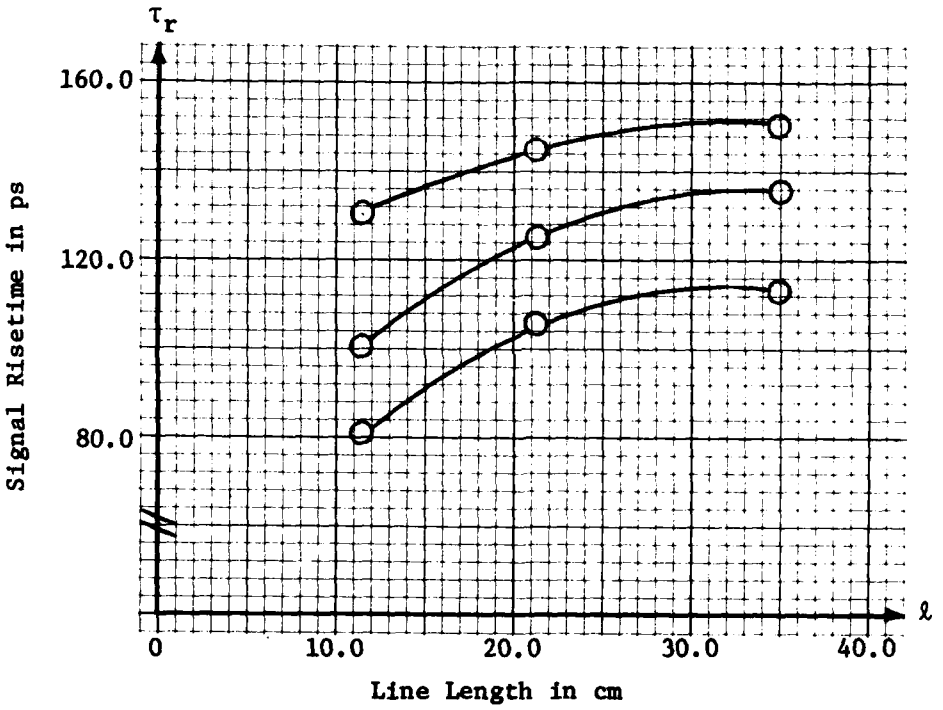

Figure 28. Signal Risetime Degradation as a Function of Line Length

6.10 Transfer Function Measurements:

From the approach discussed in Section 4.0, the data of Table 1 was calculated. Despite the attempt to eliminate the pulse width (τ_w) from the function $X(n\omega_o)$, data calculated from the measured characteristics proved otherwise. To eliminate this influence, the $X(n\omega_o)$

TABLE 1

Calculated Fourier Coefficients for the Input and Output Pulses, Values of $X(n\omega_o)$ as Calculated from Equation 44, and the Experimental and Theoretical Values of $A(n\omega_o)/k$. (A Microstrip Line Length of 20.32 cm was used.)

	Input Pulse					Output Pulse		Experimental	Theoretical
	τ_w = 500 ps		τ_w = 263 ps		τ_w = 455 ps	τ_w = 455 ps		$A(n\omega_o)/k$	$A(n\omega_o)/k$
n	a_n	$X(n\omega_o)$	a_n	$X(n\omega_o)$	$X(n\omega_o)$	a_n	$X(n\omega_o)$	$(X(n\omega_o)_{out}/X(n\omega_o)_{in})$	
0	34.47	1	20.82	1	1	26.19	1	1	1
1	66.99	.997	41.15	.988	.995	51.02	.995	1	.966
2	61.35	.988	39.67	.980	.986	47.13	.981	.995	.952
3	52.68	.981	37.31	.956	.976	41.13	.958	.982	.941
4	41.92	.955	34.21	.924	.949	33.69	.928	.978	.932
5	30.26	.933	30.54	.883	.924	25.56	.891	.964	.925
6	18.79	.901	26.51	.836	.894	17.50	.850	.950	.918
7	8.49	.875	22.31	.783	.857	10.14	.807	.942	.911
8	0	-	18.11	.724	-	3.94	.763	-	.906
9	-6.05	.810	14.09	.660	.782	-0.85	.730	.934	.900
10	-9.79	.789	10.35	.588	.750	-4.16	.682	.909	.895
11	-11.33	.768	7.00	.505	.718	-6.10	.647	.901	.890

terms for two different input pulse widths were computed and a linear interpolation made to the width of the output pulse. The interpolated values of $X(n\omega_o)_{in}$ were then used to calculate the transfer function normalized to the DC amplitude (E). This transfer function was then compared to the theoretical normalized transfer function of Equation 15. The results are plotted in Figure 29. The measured transfer function converges to the theoretical function as frequency increases. The variation at the lower frequencies can be attributed to round off errors in the computed values.

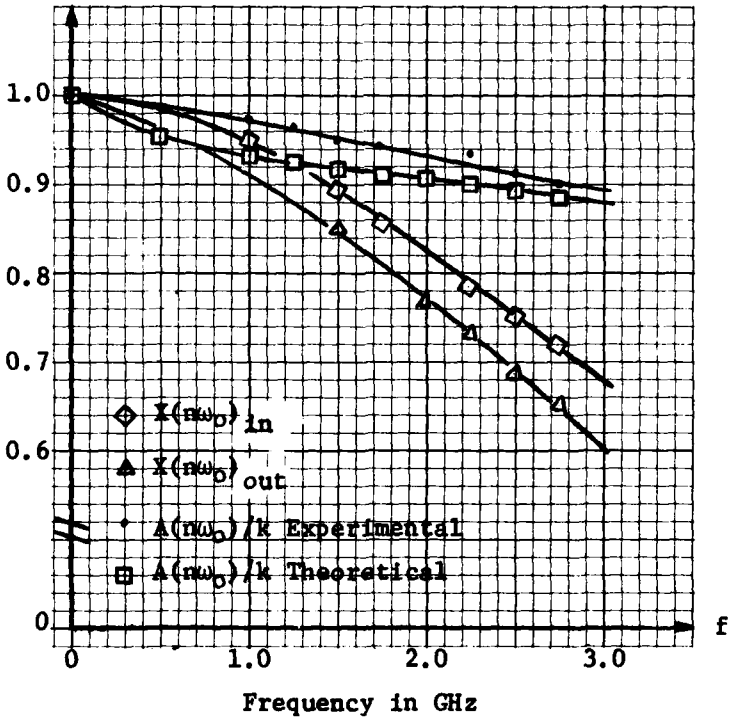

Figure 29. Experimental and Theoretical Transfer Functions of a 20.32 cm Length of 100 ohm (W = 5 mils, h = 35 mils) Microstrip. Values of $X(n\omega_o)$ as Calculated from Equation (44) are also Plotted for the Input and Output Pulses.

Using the curve fitting routine described in Section 4.0, the polynomial coefficients (b_n) were calculated for the theoretical and experimental values of $A(n\omega_o)/k$. Calculating 3 terms (second degree polynomial) the theoretical transfer function is

$$A(n\omega_o)/k = 0.9855 - 0.0590(n\omega_o) + 0.0090(n\omega_o)^2 ,$$

and the experimental transfer function is

$$A(n\omega_o)/k = 1.006 - 0.0329(n\omega_o) - 0.0022(n\omega_o)^2 .$$

These two expressions converge at approximately 2.9 GHz.

Calculating only 2 terms, the theoretical transfer function becomes

$$A(n\omega_o)/k = 0.9682 - 0.0299(n\omega_o) ,$$

and the experimental transfer function is

$$A(n\omega_o)/k = 1.0127 - 0.0376(n\omega_o) .$$

These expressions converge at approximately 6.0 GHz. It was felt the first degree polynomial gave a better approximation of the transfer functions than the higher order polynomial although the curve did not go through all the points.

To complete the calculation of the experimental transfer function, the value of k as defined by Equation 49 was calculated to be

$$k = \frac{E_{out}}{E_{in}} = 0.74 .$$

Therefore; $A(n\omega_o) = 0.8355 - 0.0278\ (n\omega_o)$.

The k value for the theoretical transfer function with $\alpha_c(0) = 0.0264$ dB/cm from Section 3.0 is

$$k = 0.94 .$$

The theoretical transfer function is then

$$A(n\omega_o) = 0.9101 - 0.0281(n\omega_o).$$

As will be noted, the theoretical and experimental expressions are very similar.

TABLE 2

COMPARISON OF SIGNAL RISETIMES USING VARIOUS RISETIME DEFINITIONS

Pulse Risetime Definition	Pulse No. 1	Pulse No. 2	Pulse No. 3
$t_r(10 - 90\%)$	93	110	122
$\frac{E}{\frac{dV}{dt}\Big\|_{max}}$	62	84	106
$\frac{E}{\frac{dV}{dt}\Big\|_{\tau_w}}$	102	117	130

6.11 Risetime Definitions:

From calculated values of a_o and values of τ_w determined by the first zero crossing of the frequency spectrum, the signal risetime was defined in three ways and results presented in Table 2. The risetime as defined in Section 4.0 by Equation (47) is approximately equal to the time it takes the pulse to go from 10% to 90% of the peak amplitude. The risetime defined from the maximum risetime rate is considerably less.

6.12 Measurements and Techniques:

All lines and line pairs were approximately 100 ohm characteristic impedance. The test equipment was 50 ohm characteristic im-

pedance. This mismatch will obviously cause errors unless eliminated. To account for the mismatch, all the signals (reference and others) were measured and characterized after they had passed through the two transitions and before the reflection from the mismatches could occur. For the transfer function measurements, the 10.16 cm line was used as a reference. For the coupling measurement, the output step function was used to determine risetime and signal amplitude. Since all transitions were identical, coupling reflections could be normalized. The results should therefore be accurate in that all signals pass through two symetrical transitions and are attenuated by the same constant.

7.0 CONCLUSIONS

The measurements in this study have shown that high impedance microstrip lines can be characterized with reasonable accuracy using the theoretical calculations presented in Section 2.0. Calculations of characteristic impedance and effective dielectric constant were within 4% of measured values. This minor variance can easily be explained by the nonuniformity of the thick film lines.

The reflection of a 70 ps risetime signal from two adjacent 90 degree bends can for all practical purposes be ignored in the design of high speed logic; however, for faster risetime signals or if several bends are on any one line, the reflected energy could cause problems. Also the effect of closely coupled lines on the characteristic impedance is relatively insignificant even down to 5 mil line to line spacing. Coupling will thus have a minor effect on the integrity of the transmitted pulse.

Coupled energy into adjacent lines will definitely be cause for concern. As would be expected from the coupling theory presented in Section 2.0, the coupling coefficients are relatively constant with changing signal risetime and with changing coupled length. Minor variations in coupling coefficients over length can be attributed to nonuniform line spacing between coupled sections. Variations in coupling coefficients as related to coupled line spacing are predictable. The backward coupling coefficients decrease significantly between 5 mil and 15 mil line spacing while the forward coupling coefficients peak around 10 mils. In the context of capacitive and inductive coupling, the backward coupled pulse is the sum of the capacitive and inductive coupled

currents, while the forward coupled pulse is the difference in the capacitive and inductive coupled currents. As the lines become close, the capacitive effect plays a more dominant role; while, as the lines become separated, the inductive coupling dominates.

The risetime degradation data plotted in Figure 28 show that all signals degrade at approximately the same rate regardless of risetime. It is felt that more data points over a wider range of risetimes and lengths would reveal more rapid degradation of the faster risetime pulses.

Determining the transfer function of high impedance microstrip lines using a fast risetime step function generator is feasible using the experimental technique defined in Section 4.0. Accuracy of the results is, however, dependent on the proper selection of data points and minimization of roundoff errors. The technique used assumes the pulse has a transform approximately equivalent to the transform of an idealized trapezoidal pulse and that the pulse width can be normalized out. It was concluded that the pulse width cannot be completely normalized out of the discrete transform; however, by interpolating between two input pulses of different widths to match the input to the output pulse width, the resulting transfer function converges to the theoretical transfer function. It was also determined from the theoretical calculations of Section 2.0 that dispersion on 100 ohm microstrip lines will be small from DC to 10 GHz and can be ignored for pulses with risetimes in the 50 ps to 150 ps range.

8.0 RELEVANCE OF RESULTS TO LOGIC DESIGNS

A rule of thumb commonly used when designing logic circuits is that 20 dB of line to line isolation should be provided to avoid crosstalk problems. This, however, will vary somewhat depending on the parameters of the actual devices being used. The isolation achieved will be a function of the line to line spacing, the length of the coupled section, and the risetime of the signals. Using the 20 dB criterion, a maximum signal risetime rate of 3.68 mV/ps and line to line spacing of 10 mils; from Figure 22, the maximum coupled length would be approximately 3 cm to avoid forward coupling problems. The 20 dB backward isolation can only be achieved by going to a line to line spacing of 14 mils (Figure 25) since reverse coupling is not a function of length.

Most logic systems use a central clock that triggers the devices and thereby synchronizes the system. Clock and signal distribution techniques as well as device switching speed will limit the operational speed of this type system. It is not likely that the degradation of pulse risetime, as caused by the interconnect line, will have any significant effect. Signal propagation delay between devices will, however, limit speed and thus the effective dielectric constant of the line is an important parameter. Attenuation of the pulses is normally not a problem providing the device threshold voltage is reached. In going to an asynchronous design where the system is timed by the propagation delay of the signals, risetime degradation could effect operation and should be taken into account.

An important reason for using high impedance interconnect lines is the reduced loading effects on the devices. This can be thought of as

either a reduction in capacitive loading or a higher impedance load depending on the risetime of the signal relative to the propagation distance between devices. This translates to a reduction in power and higher switching rates which are both very important concerns in meeting demanding operational requirements.

9.0 RECOMMENDATIONS

Only 3 data points for each of the coupling conditions were measured due to the limited number of circuits fabricated. More data points would have been very beneficial and allow more accurate assessment of results. It would also be desirable to fabricate circuits with wider lines to establish a more complete data base. Although it was determined that 5 mil lines were the smallest practical lines to fabricate using thick film technology, others have claimed success in fabricating lines as small as 2 to 3 mils. These smaller lines would be desirable for interconnecting high speed logic and should be characterized.

It would be beneficial to characterize the microstrip circuits fabricated using automatic network analysis techniques and attempt to correlate the results to the time domain measurements used in this study.

10.0 REFERENCES

1. K. C. Gupta, Ramesh Garg, and I. J. Bahl, "Microstrip Lines and Slotlines", Artech House Inc. (1979).

2. H. A. Wheeler, "Transmission Line Properties of Parallel Strips Separated by a Dielectric Sheet", IEEE Trans Microwave Theory and Techniques, Vol. MTT-13, pp 172-185 (March 1965).

3. I. J. Bahl and D. K. Trivedi, "A Designers Guide to Microstrip", Microwaves, pp 174 (May 1977).

4. R. A. Pucel, D. J. Massé and C. P. Hartwig, "Loses in Microstrip", IEEE Trans Microwave Theory and Techniques, Vol. MTT-16, pp 242-350 (June 1968). "Correction to Losses in Microstrip", Ibid (Correspondents), Vol. MTT-16, pp 1064 (December 1968).

5. E. Belohoubek, D. Denlinger, "Loss Considerations in Microstrip Resonators", IEEE Trans Microwave Theory and Techniques (June 1975).

6. George D. Vendelin, "Limitations on Stripline", Microwave Journal, Vol. 13, No. 5, pp 63-69 (May 1970).

7. W. J. Chudubiak, O. P. Jain, V. Makios, "Dispersion in Microstrip", Correspondents, IEEE Trans on Microwave Theory and Techniques, pp 783 (September 1971).

8. H. R. Kaupp, "Pulse Crosstalk Between Microstrip Transmission Lines", 7th International Electronics Packaging Symposium Record, WESCON (1966).

9. A. Papoulis, "The Fourier Integral and Its Applications", McGraw Hill (1962).

10. Charles A. Harper, Editor-in-Chief "Handbook on Thick Film Hybrid Microelectronics", McGraw Hill (1969).

11. James A. Strickland, "Time Domain Reflectometry Measurements", Tektronic Measurement Concept Series (1970).

12. Edgar J. Denlinger, "A Frequency Dependent Solution for Microstrip Transmission Lines", IEEE Transactions on Microwave Theory and Techniques, Vol. MTT-19, No. 1, pp 30-39 (January 1971).

*U.S.Government Printing Office: 1981 — 559-004/3009

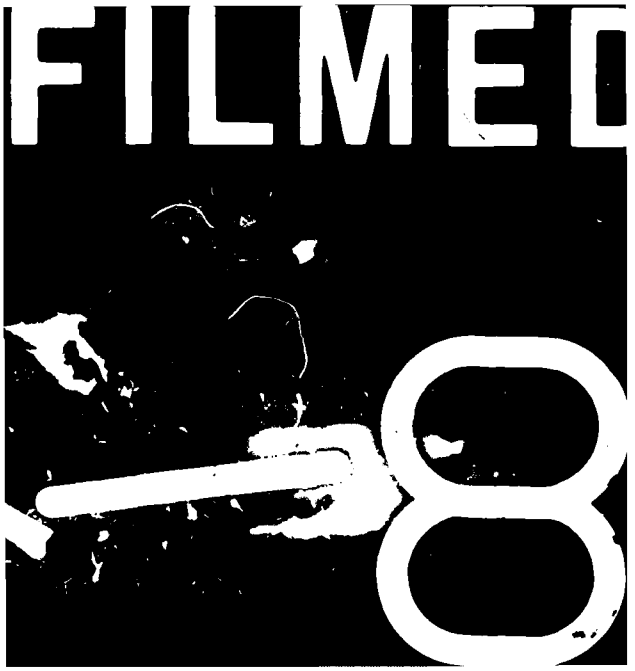
FILME
8